Analysis and Design of Low-Distortion CMOS Source Followers

Xianping Fan and P. K. Chan

***Abstract*—This paper presents the analysis of CMOS technology based nMOS source follower (NSF), pMOS source follower (PSF), and cascade-complementary source follower(CCSF) using a simplified large-signal model. Three new large-signal second harmonic equations and high-frequency transfer functions are derived. Optimization strategies which permit optimal design for low-distortion NSF, PSF, and CCSF are proposed. This includes a new complementary linearization method introduced for CCSF. With employment of dedicated optimization, the CCSF can achieve significantly better low-distortion broad-band characteristics than the other schemes. Comparative HSPICE simulated results for the three source followers have shown good agreement with the second-order analytical results using the simplified BSIM3 model equations.**

***Index Terms*—Buffer, CMOS circuit, harmonic distortion, large-signal model, linearization, source follower.**

I. Introduction

SOURCE followers are general building blocks in a large number of high-speed or high-frequency applications [1], [2] because of their intrinsic simplicity and high bandwidth characteristics. However, they suffer from several nonideal effects, including body effects, channel-length modulations, signal-dependent capacitive effects and frequency-dependent distortions arising from the capacitive load. These nonideal factors create a tradeoff between linearity, bandwidth and power consumption that present a significant design challenge. The cascode approach [3] is proven to yield high linearity but it may not be suitable for use in modern very large-scale integration (VLSI) deep-submicrometer CMOS processes with low supply voltages. Therefore, the main objective of this paper is to devise a linearized technique for source followers that allows for wide-bandwidth, low-distortion operation without a substantial increase in power consumption at a single 3-V supply.

The distortion analysis of a standard MOS source follower has been reported in [4]. This analysis is based on nonlinear parameters, g_m and $g_{\rm ds}$, in a low-frequency small-signal model. Further distortion analysis using the methods of [5], [6] extends the peculiar small-signal model with additional frequency-dependent capacitive effects, enabling the analysis of high-frequency distortion in analog integrated circuits. When the signal amplitude is increased to sufficiently high levels, the large-signal analysis approach introduced in the foundation work by [7] may be suitable because it deals directly with the nonlinear large-signal current source. Despite the fact that the analysis [7] is conducted on a low-frequency basis, the high-frequency distortion behavior of pMOS source follower (PSF) and nMOS source follower (NSF) has been addressed in recent research efforts by [8].

Thus, the second objective of this paper is to analyze and investigate the high-frequency harmonic distortion performance of the source followers using a large-signal approach. In view of the complexity introduced by including every parasitic of the large-signal model [9] in second-order analysis, a simplified approach has been adopted in this work to eliminate nondominant parasitic elements so that the ultimate model is amenable for hand analysis without losing much accuracy. This analysis is crucial because it provides significant insight as to how the process and design parameters impact the linearity of source followers under high-frequency, large-signal conditions.

Section II describes a fundamental large-signal model with frequency-dependent parasitics for an MOS transistor. A simplified model of the same is also presented along with simplified BSIM3 model equations and assumptions for the harmonic analysis. In Section III, the application of a simplified large-signal model to the derivation of the dominant second harmonic analysis and the high-frequency large-signal transfer functions of NSF, PSF, and CCSF is presented. This application illustrates how the nonlinear terms are originated and mutually subtracted in the process. In Section IV, the performance of the three source followers is observed. A case study is provided of the distortion optimization of an NSF. This is then followed by a summary of the optimization procedures for all the source followers. Concluding remarks are made in Section V.

II. Large-Signal Models and Assumptions

Fig. 1 shows a complete large-signal model for an MOS transistor [9]. The primary purpose of the diodes is to model the dc leakage currents which are small enough to be ignored in dc analysis. For ac consideration, the parasitic resistors and capacitors are key elements that determine the frequency response of the MOS transistor. In typical CMOS submicrometer technology like the 0.35-μm CMOS standard process, it can be estimated that the maximum time constant is 3.25 ps for a 10-pF capacitive load (using an example of a practical nMOS transistor layout with channel width $W = 200$ μm). Consequently, when operating in the range of a few hundred megahertz with the given technology, neglecting r_D and r_S does not cause significant inaccuracy in the prediction of the harmonics of the source fol-

Manuscript received July 2, 2004; revised November 12, 2004. This paper was recommended by Associate Editor W. A. Serdijn.

X. Fan was with the School of Electrical and Electronic Engineering, Nanyang Technological University, Singapore 639798. She is now with O_2 Micro, Singapore (e-mail: p149624457@ntu.edu.sg).

P. K. Chan is with the School of Electrical and Electronic Engineering, Nanyang Technological University, Singapore 639798 (e-mail: epkchan@ntu.edu.sg).

Digital Object Identifier 10.1109/TCSI.2005.851711

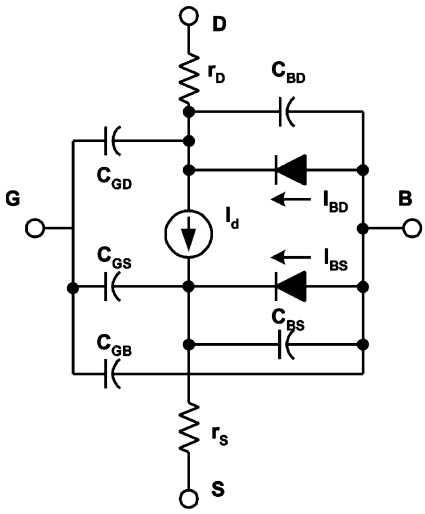

Fig. 1. Complete large-signal model for MOS transistor.

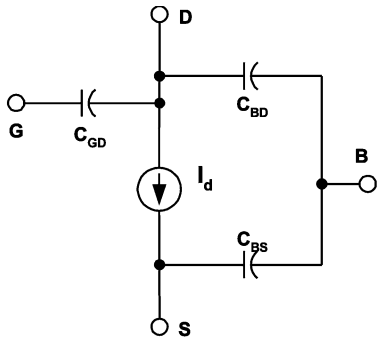

Fig. 2. Simplified large-signal model for analysis of source follower.

lowers. For parasitic capacitors consideration, $C_{\rm GB}$ can be neglected due to the shield of the inverted channel. $C_{\rm GD}$ is treated as a parasitic capacitor with a constant value when the transistor operates in the saturation region. $C_{\rm GS}$ in conjunction with the lumped output capacitive load, contributes to a feed-forward effect. However, as far as the output follows the input in source follower design and the effective output capacitive load is made dominant, $C_{\rm GS}$ can be ignored for simplification, without introducing unacceptable levels of error. Although the nonlinear junction capacitances, $C_{\rm BD}$ and $C_{\rm BS}$, are subject to signal-dependent bias, their capacitances can be treated as nominal capacitances based on nominal biasing voltage for simplified analysis. Taking into account the dominant elements mentioned, a simplified large-signal model that is suitable for the large-signal analysis of source followers is depicted in Fig. 2. In contrast to the voltage-controlled current source in the small-signal model, the current source I_d is a large-signal current source and the model includes second-order effects such as body effect, channel-length modulation, and so forth. All the transistors in the source followers are assumed to operate in saturation region.

All the equations presented in the following paragraphs refer to the nMOS transistor. In general, the subscript n denotes nMOS based parameters whilst p denotes the pMOS based counterparts. Prior to the analysis, we describe the assumptions relating to the other dominant second-order effects as follows.

A. Body Effect

Body effect occurs when the bulk potential is not equal to the source potential in an MOS transistor. This is a significant effect because of the increasing value of threshold voltage that arises through bulk modulation and the generation of a dominant second harmonic that dictates the total harmonic distortion (THD) in a large-signal condition. The threshold voltage for an nMOS transistor can be approximated as

$$V_{{\rm th}\,n} \cong V_{{\rm th}\,n0} + K1_n(\sqrt{2\Phi_{\rm fn} + V_{\rm SB}} - \sqrt{2\Phi_{\rm fn}}) \qquad (1)$$

where $V_{{\rm th}\,n0}$ is the threshold voltage when bulk is connected to source, $K1_n$ is the first-order body coefficient and $\Phi_{\rm fn}$ is the Fermi level.

B. Channel Length Modulation and Bulk Charge Effect

The channel length modulation causes error in low-frequency gain and generates harmonics. It is particularly pronounced for short channel transistors. For accurate hand analysis, the drain current using the nonideal square law equation [10] for nMOS transistors is assumed as follows:

$$I_d = \frac{k'_n W}{2L_{\rm eff} A_{{\rm bulk}\,n}}(V_{\rm GS} - V_{{\rm th}\,n})^2(1 + \lambda_n V_{\rm DS}) \qquad (2)$$

with $A_{{\rm bulk}\,n} \cong 1 + (A_{0n}K1_n)/(2\sqrt{2\Phi_{\rm fn} + V_{\rm SB}})$ and $k'_n \cong \mu_{0n}C_{\rm ox}$, where μ_{0n} is the mobility of nMOS device, $C_{\rm ox}$ is the gate capacitance per unit area, $A_{{\rm bulk}\,n}$ represents the bulk charge factor due to the nonuniform depletion region along the channel and A_{0n} is the bulk charge coefficient. For ease of hand analysis, λ_n is simplified from the BSIM3 model equations [10] as follows:

$$\lambda_n = \frac{1}{V_A} \cong \frac{1}{V_{\rm Asat} + V_{\rm ACLM}} \qquad (3)$$

with

$$\begin{aligned} V_{\rm Asat} =& E_{\rm sat}L_{\rm eff} + V_{\rm dsat}, V_{\rm ACLM} \\ =& (1/P_{\rm CLMn})(A_{{\rm bulk}\,n}E_{\rm sat}L_{\rm eff} \\ &+ (V_{\rm gs} - V_{\rm th}))/(A_{{\rm bulk}\,n}E_{\rm sat}l_n)(V_{\rm ds} - V_{\rm dsat}) \end{aligned}$$

and

$$l_n = \sqrt{(\varepsilon_{\rm si}T_{\rm ox}X_{\rm Jn})/(\varepsilon_{\rm ox})}$$

where $P_{\rm CLMn}$ is the correction factor for channel length modulation, $X_{\rm Jn}$ is the junction depth, and $E_{\rm sat}$ corresponds to the critical electrical field at which the carrier velocity becomes saturated. Since $E_{\rm sat}L_{\rm eff} \gg V_{\rm dsat}$, $A_{\rm bulk}E_{\rm sat}L_{\rm eff} \gg (V_{\rm gs} - V_{\rm th})$, and $V_{\rm ds} \gg V_{\rm dsat}$ in this application, (3) can be simplified as

$$\lambda_n = \frac{1}{V_{\rm Asat} + V_{\rm ACLM}} \cong \frac{1}{E_{\rm sat}L_{\rm eff} + \frac{1}{P_{\rm CLMn}}\frac{L_{\rm eff}}{l_n}V_{\rm ds}}. \qquad (4)$$

III. Analysis of Source Followers

A. Harmonic Distortion Analysis

The linearity of a circuit can be evaluated by the harmonic distortion. The second harmonic distortion is most significant under the large-signal condition [8]. It is typically at least several times larger than other distortion terms, so its value can be

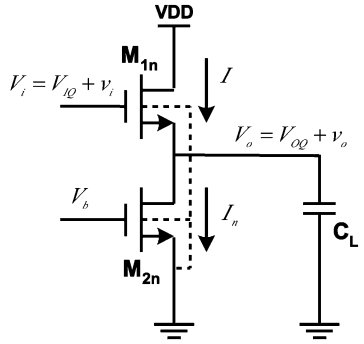

Fig. 3. NSF.

approximated as the total harmonic distortion. According to the power series expansion in [7], [11], the input–output function of a nonlinear system is normally expressed as

$$\begin{aligned} V_i &= f(V_o) \\ &= \sum_{n=0}^{\infty} \frac{f^{(n)}(V_o = V_{\rm OQ})}{n!}(V_o - V_{\rm OQ})^n \\ &= \sum_{n=0}^{\infty} b_n(v_o)v_o^n \end{aligned} \tag{5}$$

with $b_0 = f(V_o = V_{\rm OQ}), b_1 = f'(V_o = V_{\rm OQ})$ and $b_2 = (f''(V_o = V_{\rm OQ}))/(2)$, where the input voltage V_i is a function of the output voltage V_o. Since the constant b_0 is the dc input voltage, (5) can be written as

$$v_i = \sum_{n=1}^{\infty} b_n(v_o)^n = b_1 v_o + b_2 v_o^2 + b_3 v_o^3 + \cdots. \tag{6}$$

To find the harmonic distortion, (6) can be rearranged [13] as

$$v_o = \sum_{n=1}^{\infty} a_n(v_i)^n = a_1 v_i + a_2 v_i^2 + a_3 v_i^3 + \cdots. \tag{7}$$

According to (6) and (7), it can be related that $a_1 = (1/b_1)$ and $a_2 = -(b_2/b_1^3)$. Let $v_i = V_m \sin\omega t$, where V_m is the peak amplitude of input signal. We have $v_o = a_1 V_m \sin\omega t + a_2(V_m \sin\omega t)^2 + \cdots$. Thus, the second harmonic distortion of a nonlinear system is obtained as [14]

$$\mathrm{HD}_2 \cong \frac{1}{2}\frac{a_2}{a_1}V_m = \frac{1}{2}\frac{b_2}{b_1^2}V_m. \tag{8}$$

1) nMOS Source Follower: The NSF in Fig. 3 consists of an nMOS input transistor and an nMOS current source that drives a capacitive load C_L. The composite input signal V_i consists of the dc biasing voltage $V_{\rm IQ}$ and the ac signal v_i, whereas the composite output signal V_o consists of the dc biasing voltage $V_{\rm OQ}$ and the ac signal v_o. For n-well CMOS process, the bulks of nMOS transistors M_{1n} and M_{2n} are shared with the same substrate. As a result, the NSF suffers from a body effect. Distortion analysis [7] based on a low-frequency model is well established to reveal a nonlinear bulk modulation term. However, this may not be adequate for broad bandwidth source followers, in which both capacitive load current as well as bulk charge effects contribute additional distortion terms.

Using the input and output notations while applying the simplified large-signal model (Fig. 2) to NSF in Fig. 3 yields the equivalent circuit of Fig. 4(a). With further simplification, Fig. 4(a) in turn leads to Fig. 4(b), where the equivalent capacitive load is $C_{{\rm Leq}\,n} = C_L + C_{{\rm BS1}n} + C_{{\rm BD2}n} + C_{{\rm GD2}n}$. The ac current passing through the capacitive load $C_{{\rm Leq}\,n}$ is $j\omega C_{{\rm Leq}\,n}(V_o - V_{\rm OQ})$. It will be significant when the circuit operates at high frequency. As a result, the input transistor M_{1n} conducts a summed current of $I = I_n + I_{\rm cn}$, with I_n and $I_{\rm cn}$ representing the dc biasing current and the frequency-dependent capacitive load current respectively. Using (2) and the prior defined terms in Fig. 4, the relationship between the currents in the transistors and capacitive load can be approximated as

$$\begin{aligned} I_n &= I - I_{\rm cn} \\ &\cong \frac{1}{2}\frac{k_n'(W/L_{\rm eff})_{1n}(V_{\rm GS1} - V_{{\rm th}\,n})^2}{A_{{\rm bulk}\,n}} \\ &\quad - j\omega C_{{\rm Leq}\,n}(V_o - V_{\rm OQ}) \end{aligned} \tag{9}$$

with $V_{{\rm th}\,n} \cong V_{{\rm th}\,n0} + K1_n(\sqrt{2\Phi_{\rm fn} + V_o} - \sqrt{2\Phi_{\rm fn}}), A_{{\rm bulk}\,n} \cong 1 + (A_{0n}K1_n)/(2\sqrt{2\Phi_{\rm fn} + V_o})$. It is noted that the channel length modulation is ignored because the nonlinearities arising from the body effect are dominated in NSF. From the definition of $V_{\rm GS1} = V_i - V_o$, (9) can be rewritten in a form as

$$\begin{aligned} V_i =& f(V_o) \\ =& V_o + V_{{\rm th}\,n0} + K1_n(\sqrt{2\Phi_{\rm fn} + V_o} - \sqrt{2\Phi_{\rm fn}}) \\ &+ \Delta V_n \sqrt{A_{{\rm bulk}\,n}\left[1 + \frac{j\omega C_{{\rm Leq}\,n}}{I_n}(V_o - V_{\rm OQ})\right]} \end{aligned} \tag{10}$$

where $\Delta V_n = \sqrt{(2I_n)/(k_n'(W/L_{\rm eff})_{1n})}$ is the fundamental first-order gate-overdrive voltage of the input transistor. As can be seen in the fourth item of (10), the second-order effect contributed by the bulk charge factor $A_{{\rm bulk}\,n}$ and the frequency-dependent capacitive item becomes a multiplication function for the gate over-drive voltage. It is reasonable because the capacitive current modulates the gate-overdrive voltage at high frequency. From (8) and (10), the second harmonic distortion of NSF is approximated as shown in (11) at the bottom of the page (see Appendix A), where $A_{{\rm bulk}\,n\_Q}$ is defined as the bulk charge factor when $V_o = V_{\rm OQ}$. In the numerator of (11), there are three nonideal terms arising from second-order effects. The first body effect term is caused by the fundamental modulation of the threshold voltage. The

$$\mathrm{HD}_{2\_\mathrm{NSF}} \cong \frac{\frac{-K1_n}{16(2\Phi_{\rm fn}+V_{\rm OQ})^{3/2}} + \frac{\Delta V_n A_{{\rm bulk}\,n\_Q}^{1/2}}{16}\left(\frac{\omega C_{{\rm Leq}\,n}}{I_n}\right)^2 + \frac{\Delta V_n K1_n A_{0n}}{32 A_{{\rm bulk}\,n\_Q}^{1/2}(2\Phi_{\rm fn}+V_{\rm OQ})^{3/2}}\left[\frac{3}{2(2\Phi_{\rm fn}+V_{\rm OQ})} - \frac{j\omega C_{{\rm Leq}\,n}}{I_n}\right]}{\left[1 + \frac{K1_n}{2(2\Phi_{\rm fn}+V_{\rm OQ})^{1/2}}\right]^2} V_m \tag{11}$$

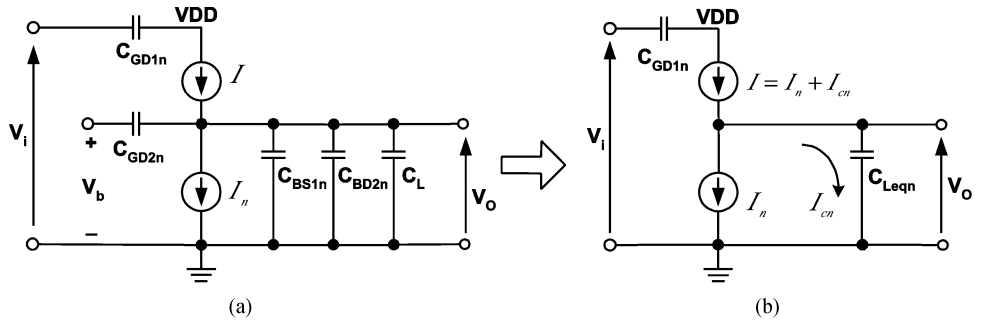

Fig. 4. Simplified large-signal model of NSF. (a) Equivalent circuit. (b) Simplified equivalent circuit.

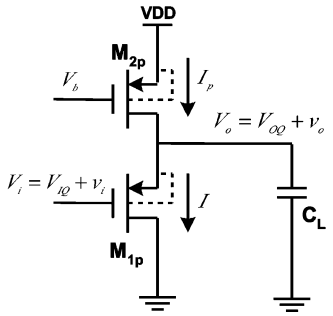

Fig. 5. PSF.

second gate-overdrive term is linked to the capacitive load, with frequency-dependent characteristics. The third term is related to the cross-product term contributed by the interaction between the first and second terms. Thus, the third term is usually small when compared to the others. At low frequencies, the second distortion term is relatively small and the harmonic distortion is dominated by the body effect term, $(-K1_n)/(16(2\Phi_{\rm fn}+V_{\rm OQ})^{3/2})$. However, with increasing frequency, the magnitude of the second frequency-dependent distortion term in (11) becomes more pronounced. As this significant term $(\Delta V_n/16)A_{{\rm bulk}\,n\_Q}^{1/2}((\omega C_{{\rm Leq}\,n})/I_n)^2$ has the opposite sign to that of the major $(-K1_n)/(16(2\Phi_{\rm fn}+V_{\rm OQ})^{3/2})$ term, the frequency-dependent distortion tends to counteract the body effect distortion at high frequency. Therefore, minimum harmonic distortion can be obtained at an optimum spot frequency.

2) pMOS Source Follower: When dealing with the circuit of a PSF, it can be seen that most designs [8], [15] have utilized a body-tied pMOS input transistor to remove the bulk modulation based distortion and to improve the precision issue. However, the transconductance efficiency is low in PSFs, resulting in a small drive ability and a larger silicon area.

Fig. 5 shows a conventional PSF in an n-well CMOS process which includes a pMOS input transistor and a pMOS current source. By applying the simplified large-signal model of Fig. 2 and introducing extra bulk-well capacitance to PSF in Fig. 5, we get Fig. 6(a). Fig. 6(b) is derived by further simplification where the equivalent capacitive load is $C_{{\rm Leq}\,p}=C_L+C_{{\rm BD1}p}+C_{{\rm BD2}p}+C_{{\rm GD2}p}+C_{w1p}$, and C_{w1p} is the bulk-well capacitance of M_{1p}. Similar to NSF, the current passing through the capacitive load $C_{{\rm Leq}\,p}$ cannot be ignored at high frequency. Hence, the input transistor M_{1p} conducts a current of $I=I_p-I_{\rm cp}$, where I_p and $I_{\rm cp}$ represent the dc biasing current and the frequency-dependent capacitive load current respectively. It is noted that $I_{\rm cp}$ is equal to $j\omega C_{{\rm Leq}\,p}(V_o-V_{\rm OQ})$ whereas I_p is $I_{p0}[1+\lambda_{2p}(V_{\rm DD}-V_o)]$ due to the channel length modulation of M_2, where I_{p0} represents the biasing current at quiescent point. In Fig. 6(b), the relationship between the currents in the transistors and the capacitive load can be established as

$$\begin{aligned} I_{p0}&[1+\lambda_{2p}(V_{\rm DD}-V_o)] \\ &= I+I_{\rm cp} \\ &\cong \frac{1}{2}\frac{k'_p(W/L_{\rm eff})_{1p}(V_{\rm SG1}-V_{{\rm th}\,p0})^2}{A_{{\rm bulk}\,p}} \\ &\quad\times(1+\lambda_{1p}V_o)+j\omega C_{{\rm Leq}\,p}(V_o-V_{\rm OQ}) \end{aligned} \tag{12}$$

where

$$\lambda_{1p}\cong\frac{1}{E_{\rm sat}L_{1p\,\rm eff}+\frac{L_{1p\,\rm eff}}{P_{{\rm CLM}\,p}l_p}V_o}\quad\text{and}$$
$$\lambda_{2p}\cong\frac{1}{E_{\rm sat}L_{2p\,\rm eff}+\frac{L_{2p\,\rm eff}}{P_{{\rm CLM}\,p}l_p}(V_{\rm DD}-V_o)}$$

are the channel-length modulation factors for M_1 and M_2 respectively and $A_{{\rm bulk}\,p}\cong 1+(A_{0p}K1_p)/(2\sqrt{2\Phi_{\rm fp}})$. From the definition of $V_{\rm SG1}=V_o-V_i$, the input voltage on the basis of (12) can be expressed as (13) shown at the bottom of the page, where $\Delta V_p=\sqrt{(2I_{p0})/(k'_p(W/L_{\rm eff})_{1p})}$ is the first-order gate-overdrive voltage of the input transistor. Like the gate-overdrive terms (10) in NSF that include the usual bulk charge factor and frequency-dependent capacitive term, the multiplication function is further complicated with additional channel-length modulation factors as observed in the third item in (13). Using routine analysis to find the respective coefficients for b_1 and b_2, and

$$V_i=f_p(V_o)=V_o-V_{{\rm th}\,p0}-\Delta V_p\sqrt{\frac{A_{{\rm bulk}\,p}[1+\lambda_{2p}(V_{\rm DD}-V_o)]-\frac{j\omega C_{{\rm Leq}\,p}}{I_{p0}}(V_o-V_{\rm OQ})}{1+\lambda_{1p}V_o}} \tag{13}$$

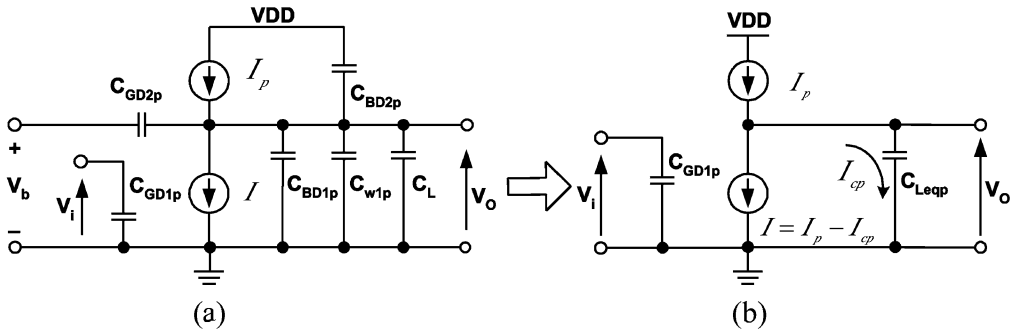

Fig. 6. Simplified large-signal model of PSF. (a) Equivalent circuit. (b) Simplified equivalent circuit.

applying the second harmonic distortion definition (8), the following equation is derived (see Appendix B):

$$\begin{aligned}
&\mathrm{HD}_{2_\mathrm{PSF}} \\
&\cong \frac{\Delta V_p\sqrt{A_{\mathrm{bulk}\,p}}}{16}V_m\left\{\frac{4}{P_{\mathrm{CLM}p}}\frac{L_{1p\,\mathrm{eff}}}{l_p}(E_{\mathrm{sat}}L_{1p\,\mathrm{eff}}\lambda_{1pQ})\right. \\
&\quad\times\left(\lambda_{1pQ}^2-\lambda_{2pQ}^2\frac{\lambda_{2pQ}}{\lambda_{1pQ}}\frac{L_{2p\,\mathrm{eff}}^2}{L_{1p\,\mathrm{eff}}^2}\right) \\
&\quad+(\lambda_{2pQ}E_{\mathrm{sat}}L_{2p\,\mathrm{eff}})^2\left(3\lambda_{1pQ}^2\frac{L_{1p\,\mathrm{eff}}}{L_{2p\,\mathrm{eff}}}-\lambda_{2pQ}^2\right) \\
&\quad+(\lambda_{1pQ}E_{\mathrm{sat}}L_{1p\,\mathrm{eff}})^2\left(3\lambda_{1pQ}^2-\lambda_{2pQ}^2\frac{L_{2p\,\mathrm{eff}}}{L_{1p\,\mathrm{eff}}}\right) \\
&\quad+\left(\frac{\omega C_{\mathrm{Leq}\,p}}{I_{p0}}\right)^2+2\frac{j\omega C_{\mathrm{Leq}\,p}}{I_{p0}} \\
&\quad\left.\times E_{\mathrm{sat}}L_{1p\,\mathrm{eff}}\left(\lambda_{1pQ}^2-\lambda_{2pQ}^2\frac{L_{2p\,\mathrm{eff}}}{L_{1p\,\mathrm{eff}}}\right)\right\}. \qquad (14)
\end{aligned}$$

Note that $\lambda_{1pQ}, \lambda_{2pQ}$ are the constant values for λ_{1p} and λ_{2p} respectively when $V_o = V_{\mathrm{OQ}}$. The appearance of the squared lambda terms stems from the double differentiation of (13) to obtain the coefficient b_2 according to (5) and the definition of (8). From (14), the second harmonic distortion of PSF is now governed by the channel length modulation and frequency-dependent factor. At low frequency, the frequency-dependent terms are negligible such that the channel length modulation terms become dominant. The harmonic distortion of PSF is expected to attain a low value because of the subtraction from the finite channel length modulation terms $\alpha_i\lambda_{1pQ}^2 - \beta_j\lambda_{2pQ}^2$ arising from two pMOS transistors, where α_i and β_j denote the respective constants for individual squared lambdas. It is also observed that the $\mathrm{HD}_{2\_\mathrm{PSF}}$ is basically the sum of all corresponding difference of squared lambda terms having first-order coefficient $(E_{\mathrm{sat}}L_{1p\,\mathrm{eff}}\lambda_{1pQ})$ and higher order coefficients $(E_{\mathrm{sat}}L_{1p\,\mathrm{eff}}\lambda_{1pQ})^2$ and $(E_{\mathrm{sat}}L_{2p\,\mathrm{eff}}\lambda_{2pQ})^2$. The PSF exhibits better linearity than the NSF because the lambda-based terms are smaller than bulk modulation terms at low frequency. However, at higher frequency, the dominant frequency-dependent term $((\omega C_{\mathrm{Leq}\,p})/I_{p0})^2$ will swamp the finite values of the lambda-based terms, and so the harmonic distortion increases monotonically with frequency. Contrasting with the NSF, there will be no optimal point using frequency-based optimization strategies. Instead, low distortion PSF is resorted to for the optimization of the channel length modulation factor through the quiescent biasing voltage V_{OQ}.

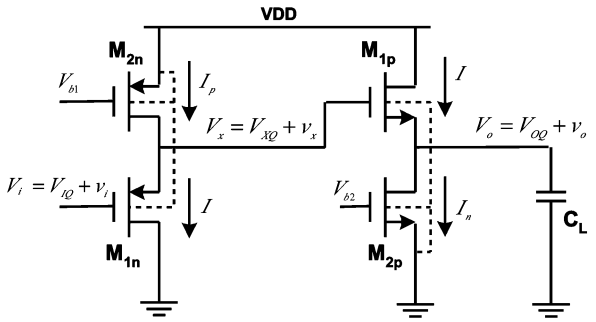

Fig. 7. CCSF.

3) Cascade-Complementary Source Follower: A cascaded source follower structure can be implemented in two possible forms: a cascade of PSF and NSF or a cascade of NSF and PSF. Their usual common goal is to alleviate the level shift problem arising from a single source follower stage. However, based on the analytical results of the prior NSF, a possibility arises of optimizing low-distortion CCSF—one that has never been reported so far. Intuitively, the new linearization method is achieved by generating the intentional body effect and frequency-dependent effect from the bulk-modulated PSF (M_{1p}, M_{2p}), with the bulks being tied to the supply instead of being self-tied to the respective source in the first stage. This will compensate for those of the nonlinear terms of NSF (M_{1n}, M_{2n}) with the common substrate serving as the bulk in the second stage as shown in Fig. 7. The NSF in CCSF is arranged in the final stage because it has higher drive ability and bandwidth than its PSF counterpart.

The equivalent circuit of Fig. 7 is illustrated in Fig. 8(a) and its simplification using a large-signal model is shown in Fig. 8(b). It is noted that the equivalent capacitive load for NSF is $C_{\mathrm{Leq}\,n} = C_L + C_{\mathrm{BS1}n} + C_{\mathrm{BD2}n} + C_{\mathrm{GD2}n}$ and the equivalent capacitive load for PSF is $C_{\mathrm{Leq}\,p} = C_{\mathrm{BS1}p} + C_{\mathrm{BD2}p} + C_{\mathrm{GD2}p} + C_{\mathrm{GD1}n}$. The capacitive load of NSF is usually dominated by the linear load C_L whereas the capacitive load of PSF is governed by the sum of nonlinear junction capacitances. As can be seen in Figs. 7 and 8(b), the input transistor M_{1n} conducts a summed current of $I = I_n + I_{\mathrm{cn}}$. The composite signal V_x consists of the dc biasing voltage V_{XQ} and the ac signal v_x. Hence, similar to (10), the input-output relationship of NSF can be expressed as

$$\begin{aligned}
V_x = V_o + V_{\mathrm{th}\,n0} + K1_n(\sqrt{2\Phi_{\mathrm{fn}}+V_o}-\sqrt{2\Phi_{\mathrm{fn}}}) \\
+\Delta V_n\sqrt{A_{\mathrm{bulk}\,n}\left[1+\frac{j\omega C_{\mathrm{Leq}\,n}}{I_n}(V_o-V_{\mathrm{OQ}})\right]}. \qquad (15)
\end{aligned}$$

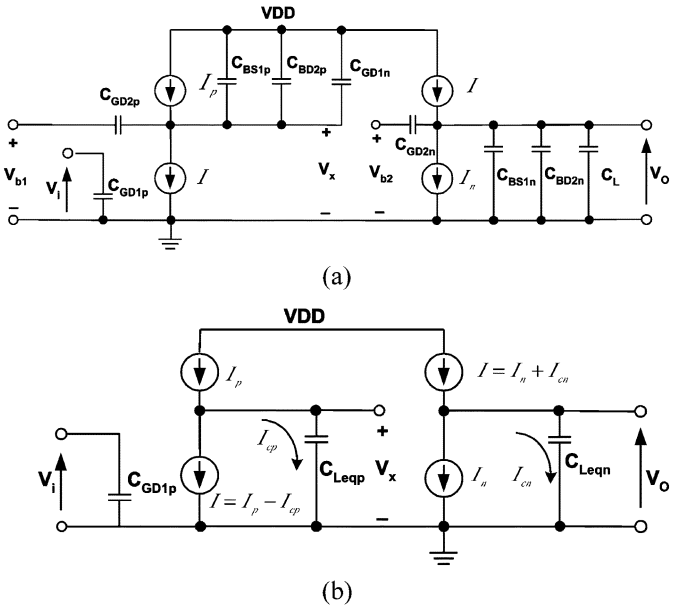

Fig. 8. Large-signal model of CCSF. (a) Equivalent circuit. (b) Simplified equivalent circuit.

For PSF, the input transistor M_{1p} conducts a current of $I = I_p - I_{\rm cp}$. Similar to (13), the input–output relationship of PSF can be expressed as

$$V_i = V_x - V_{{\rm th}p0} - K1_p\left(\sqrt{2\Phi_{\rm fp} + (V_{\rm DD} - V_x)} - \sqrt{2\Phi_{\rm fp}}\right) - \Delta V_p\sqrt{A_{{\rm bulk}p}\left[1 - \frac{j\omega C_{{\rm Leq}p}}{I_p}(V_x - V_{\rm XQ})\right]} \quad (16)$$

where $A_{{\rm bulk}n}$ is given in the prior NSF analysis and $A_{{\rm bulk}p} \cong 1 + (A_{0p}K1_p)/(2\sqrt{2\Phi_{\rm fp} + V_{\rm DD} - V_x})$ for pMOS transistor. Since the expansion of the square-root based V_x terms in (16) would be small, it can be replaced with the first-order approximated V_x term from (15), with $V_x \cong V_o + V_{\rm GS\_Q}$ and $V_{\rm GS\_Q} = V_{{\rm th}n0} + K1_n(\sqrt{2\Phi_{\rm fn} + V_{\rm OQ}} - \sqrt{2\Phi_{\rm fn}}) + \Delta V_n\sqrt{A_{{\rm bulk}n}}$. Substituting the V_x (15) into the first term of (16) and the approximated V_x term into the square root terms of (16), we obtain

$$\begin{aligned} V_i = {} & V_o + V_{{\rm th}n0} + K1_n\left(\sqrt{2\Phi_{\rm fn} + V_o} - \sqrt{2\Phi_{\rm fn}}\right) \\ & + \Delta V_n\sqrt{A_{{\rm bulk}n}\left[1 + \frac{j\omega C_{{\rm Leq}n}}{I_n}(V_o - V_{\rm OQ})\right]} \\ & - V_{{\rm th}p0} - K1_p\left(\sqrt{2\Phi_{\rm fp} + [V_{\rm DD} - (V_o + V_{\rm GS\_Q})]} - \sqrt{2\Phi_{\rm fp}}\right) \\ & - \Delta V_p\sqrt{A_{{\rm bulk}p}\left[1 - \frac{j\omega C_{{\rm Leq}p}}{I_p}(V_o + V_{\rm GS\_Q} - V_{\rm XQ})\right]}. \end{aligned} \quad (17)$$

From our routine analysis as described before, the second harmonic distortion of CCSF is as shown in (18) at the bottom of the page (see Appendix C). From (18), similar to NSF, the CCSF includes nonlinearities due to the bulk modulation of threshold voltage, the gate-overdrive term with the frequency-dependent effect via capacitive load and the non-dominant cross-product term linked to the former items. All items in the numerator caused by the NSF have their corresponding counterparts with opposite signs generated by the PSF. The low-distortion optimization strategy can be formulated by (i) minimizing the summed value of the dominant frequency-independent pair, $-(K1_n)/(16(2\Phi_{\rm fn} + V_{\rm OQ})^{3/2})$ and $+(K1_p)/(16[2\Phi_{\rm fp} + (V_{\rm DD} - V_{\rm OQ} - V_{\rm GS\_Q})]^{3/2})$, by finding the optimum $V_{\rm OQ}$, and by (ii) minimizing the summed value of the dominant frequency-dependent pair, $+(\Delta V_n A_{{\rm bulk}n\_Q}^{1/2})/(16)((\omega C_{{\rm Leq}n})/(I_n))^2$ and $-(\Delta V_p A_{{\rm bulk}p\_Q}^{1/2})/(16)((\omega C_{{\rm Leq}p})/(I_p))^2$, by finding the optimum $C_{{\rm Leq}p}$ or $C_{{\rm Leq}n}$ for balance cancellation.

B. Large-Signal Transfer Function

Based on the input and output signals defined as $V_i = V_{\rm IQ} + v_i$ and $V_o = V_{\rm OQ} + v_o$, $V_i = f(V_o)$ can be rewritten as

$$\begin{aligned} v_i = {} & -V_{\rm IQ} + f(V_o) \\ \cong {} & -V_{\rm IQ} + f(V_o = V_{\rm OQ}) + f^{(1)}(V_o = V_{\rm OQ})v_o. \end{aligned} \quad (19)$$

$$\begin{aligned} & -\frac{K1_n}{16(2\Phi_{\rm fn} + V_{\rm OQ})^{3/2}} + \frac{\Delta V_n A_{{\rm bulk}n\_Q}^{1/2}}{16}\left(\frac{\omega C_{{\rm Leq}n}}{I_n}\right)^2 \\ & + \frac{\Delta V_n K1_n A_{0n}}{64A_{{\rm bulk}n\_Q}^{1/2}(2\Phi_{\rm fn} + V_{\rm OQ})^{3/2}}\left(\frac{3}{(2\Phi_{\rm fn} + V_{\rm OQ})} - \frac{2j\omega C_{{\rm Leq}n}}{I_n}\right) \\ & + \frac{K1_p}{16[2\Phi_{\rm fp} + (V_{\rm DD} - V_{\rm OQ} - V_{\rm GS\_Q})]^{3/2}} - \frac{\Delta V_p A_{{\rm bulk}p\_Q}^{1/2}}{16}\left(\frac{\omega C_{{\rm Leq}p}}{I_p}\right)^2 \\ & - \frac{\frac{\Delta V_p K1_p A_{0p}}{64A_{{\rm bulk}p\_Q}^{1/2}[2\Phi_{\rm fp} + (V_{\rm DD} - V_{\rm OQ} - V_{\rm GS\_Q})]^{5/2}}\left(\frac{3}{[2\Phi_{\rm fp} + (V_{\rm DD} - V_{\rm OQ} - V_{\rm GS\_Q})]} - \frac{2j\omega C_{{\rm Leq}p}}{I_p}\right)}{\left(1 + \frac{K1_n}{2(2\Phi_{\rm fn} + V_{\rm OQ})^{1/2}} + \frac{K1_p}{2[2\Phi_{\rm fp} + (V_{\rm DD} - V_{\rm OQ} - V_{\rm GS\_Q})]^{1/2}}\right)^2} V_m \end{aligned} \quad (18)$$

Since, $f(V_o = V_{\rm OQ}) = V_{\rm IQ}$, the large signal transfer function can be expressed as

$$H = \frac{v_o}{v_i} \cong \frac{1}{f^{(1)}(V_o = V_{\rm OQ})}. \tag{20}$$

For NSF, according to (10) and (20), the large-signal transfer function of NSF becomes (21) shown at the bottom of the page. For PSF, according to (13) and (20), the large-signal transfer function is (22) shown at the bottom of the page. For CCSF, from (17) and (20), the large-signal transfer function is obtained as (23) shown at the bottom of the page. From (21), the voltage gain of the NSF is smaller than 1, and the gain error is a complex number. The real portion is mainly contributed by the body effect term $(K1_n)/(2(2\Phi_{\rm fn} + V_{\rm OQ})^{1/2})$ that is independent of frequency, whereas the imaginary portion is caused by the frequency-dependent term $((\Delta V_n A_{{\rm bulk}\,n\_Q}^{1/2})/2)(j\omega C_{{\rm Leq}\,n})/(I_n)$ that is significant at high frequency. Thus, the large-signal gain exhibits dc gain error at low frequency and it rolls off at high frequency. Due to the minute channel length modulation terms in (22), the low-frequency gain of PSF is much closer to 1 than that of NSF in (21). As in the NSF, the channel-length modulation term is responsible for the real portion whilst the frequency-dependent term is responsible for the imaginary portion. When operation frequency is increased to high levels, the frequency-dependent term in the imaginary portion becomes significant. From (23), the low frequency gain error of CCSF is larger than that of the NSF in (21) and PSF in (22) due to the summation of the body effects in NSF and PSF. This can be regarded as a disadvantage of the scheme. At high frequencies, the gain decreases because the frequency-dependent effect becomes apparent.

IV. Results and Discussions

The process and design parameters used in hand calculations to predict the second harmonic distortion results are shown in Tables I and II, respectively. As the second-order distortion component is much larger than the third and fourth harmonics under large signal conditions, the second harmonic is very close to the THD. The THD is therefore used to denote the linearity of the three source followers in simulation whilst maintaining reasonable accuracy. In order to verify the second-order analytical result and compare the relative linearity performance, the THD of NSF, PSF, and CCSF were simulated using realistic Level 49 BSIM3 models from 0.35-μm CMOS process technology.

A. Performance of Source Followers

For low-frequency verification, the input frequency was chosen such that the frequency-dependent distortion components are not of any significant impact and the harmonic distortion is governed by the frequency-independent nonlinearities. According to the prior analysis, these frequency-independent nonlinear terms are functions of quiescent operation points. Fig. 9 shows the variation of the THD of NSF, PSF, and CCSF against different $V_{\rm OQ}$ at 10 MHz. In relation to the NSF, the THD is decreased because the major bulk modulated component $(-K1_n)/(16(2\Phi_{\rm fn} + V_{\rm OQ})^{3/2})$ decreases with increasing $V_{\rm OQ}$ as revealed in (11). For the PSF, the distortion characteristic appears as a V-shaped function against the change of $V_{\rm OQ}$. This observation is consistent with the observation in (14) that it results from the mutual subtraction of the bias-dependent channel length modulation terms $(\lambda_{1pQ}, \lambda_{2pQ})$ from the input transistor and biasing transistor, with the degree of subtraction controlled by $V_{\rm OQ}$. For the CCSF, the minimum THD can also be observed at a particular output quiescent voltage bias point because of the involvement of a PSF that has a similar V-shaped function. The optimum distortion point arises from the cancellation between pMOS and nMOS based body effect terms, with dominant components denoted as $(-K1_n)/(16(2\Phi_{\rm fn} + V_{\rm OQ})^{3/2})$ and $(K1_p)/(16[2\Phi_{\rm fp} + (V_{\rm DD} - Vf_{\rm OQ} - V_{{\rm GS}\_Q})]^{3/2})$ in (18). This allows the CCSF to get low distortion at low frequencies.

For high-frequency verification, all the source followers should start with optimum quiescent bias prior to investigating the high-frequency distortion characteristics. Because there is no formal optimal bias point in NSF as described above, the $V_{\rm OQ}$ is preferably set at half the supply voltage. The $V_{\rm OQ}$ of the PSF and CCSF are based on the optimized values according to Fig. 9. The simulated high-frequency THD characteristics of PSF, NSF and CCSF together with the calculated results

$$H_{\rm NSF} \cong \frac{1}{1 + \frac{K1_n}{2(2\Phi_{\rm fn}+V_{\rm OQ})^{1/2}} - \frac{\Delta V_n}{8A_{{\rm bulk}\,n\_Q}^{1/2}} \frac{K1_n A_{0n}}{(2\Phi_{\rm fn}+V_{\rm OQ})^{3/2}} + \frac{\Delta V_n A_{{\rm bulk}\,n\_Q}^{1/2}}{2} \frac{j\omega C_{{\rm Leq}\,n}}{I_n}} \tag{21}$$

$$H_{\rm PSF} \cong \frac{1}{1 + \frac{\Delta V_p \sqrt{A_{{\rm bulk}\,p}}}{2} \left\{ \lambda_{2pQ}^2 E_{\rm sat} L_{2p\,\rm eff} + \lambda_{1pQ}^2 E_{\rm sat} L_{1p\,\rm eff} + \frac{j\omega C_{{\rm Leq}\,p}}{I_{p0}} \right\}} \tag{22}$$

$$\begin{aligned} H_{\rm CCSF} \cong \frac{1}{1 + \dfrac{K1_n}{2(2\Phi_{\rm fn} + V_{\rm OQ})^{1/2}} + \dfrac{K1_p}{2[2\Phi_{\rm fp} + (V_{\rm DD} - V_{\rm OQ} - V_{{\rm GS}\_Q})]^{1/2}} \\ + \frac{\Delta V_n}{2A_{{\rm bulk}\,n\_Q}^{1/2}} \left(\frac{-K1_n A_{0n}}{4(2\Phi_{\rm fn} + V_{\rm OQ})^{3/2}} + A_{{\rm bulk}\,n\_Q} \frac{j\omega C_{{\rm Leq}\,n}}{I_n} \right) \\ + \frac{\Delta V_p}{2A_{{\rm bulk}\,p\_Q}^{1/2}} \left(\frac{-K1_p A_{0p}}{4[2\Phi_{\rm fp} + (V_{\rm DD} - V_{\rm OQ} - V_{{\rm GS}\_Q})]^{3/2}} + A_{{\rm bulk}\,p\_Q} \frac{j\omega C_{{\rm Leq}\,p}}{I_p} \right) \end{aligned} \tag{23}$$

TABLE I
PROCESS PARAMETERS USED IN HAND CALCULATIONS

NMOS Process Parameter	Value	PMOS Process Parameter	Value
$V_{thn0}(V)$	0.5	$V_{thp0}(V)$	0.69
$K1_n(V^{1/2})$	0.5	$K1_p(V^{1/2})$	0.6
$\mu_{0n}(m^2/V\sec)$	$4.758*10^{-2}$	$\mu_{0p}(m^2/V\sec)$	$1.482*10^{-2}$
$T_{ox}(m)$	$7.575*10^{-9}$	$T_{ox}(m)$	$7.754*10^{-9}$
P_{CLMn}	0.695	P_{CLMp}	3.184

TABLE II
DESIGN PARAMETERS USED IN HAND CALCULATIONS

Design Parameter At supply $V_{dd}=3$V	PSF	NSF	CCSF	
	PMOS bulk tied to source		PSF with PMOS bulk tied to V_{dd}	NSF in CCSF
Biasing Current	1 mA	1mA	0.1 mA	1 mA
Input Transistor (W)	500 μm	200 μm	40 μm	200 μm
Input Transistor (L_{eff})	0.49 μm	0.45 μm	0.49 μm	0.45 μm
Biasing Transistor (W)	60 μm	60 μm	10 μm	60 μm
Biasing Transistor (L_{eff})	0.49 μm	0.45 μm	0.49 μm	0.45 μm
Bulk-well Capacitance	0.25 pF	-	-	-

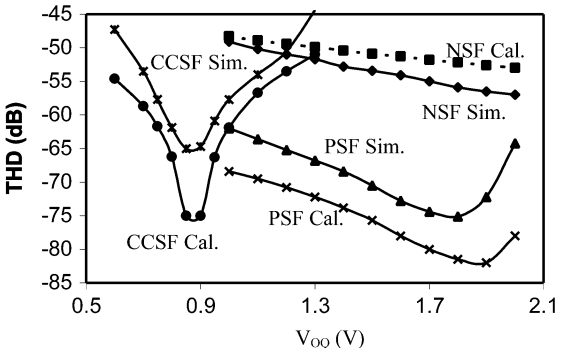

Fig. 9. THD versus $V_{\rm OQ}$ at 1 $V_{\rm PP}$ input, 1-pF load and 10-MHz input frequency.

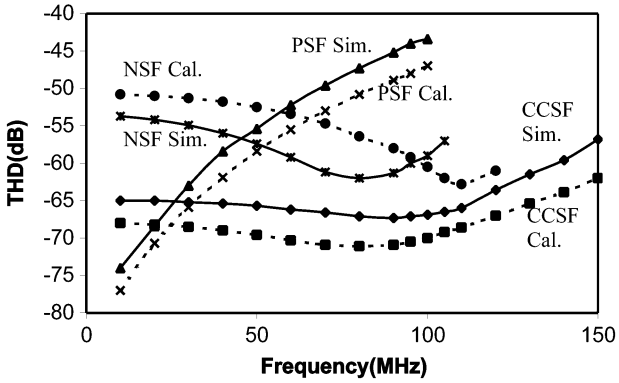

Fig. 10. THD characteristic of CCSF at high frequency and its THD comparison with NSF and PSF based on 1 $V_{\rm PP}$ input, 1 pF load and optimal $V_{\rm OQ}$ among the three schemes.

are illustrated in Fig. 10. For PSF, THD exhibits the highest linearity at low frequency because of the elimination of the body effect and because there is negligible contribution from the high-frequency nonlinear factor. However, the linearity degrades progressively with increasing the input frequency. This confirms that the dominant frequency-dependent term $((\omega C_{\rm Leq}p)/I_{p0})^2$ overrides the minute channel length modulation terms in (14). For NSF, although it displays the relative higher nonlinearity at low frequency due to a strong body effect, the nonlinear effect is progressively compensated with the increase in frequency. The view that the frequency-dependent distortion component $(\Delta V_n)/(16)A^{1/2}_{{\rm bulk}\,n\_Q}((\omega C_{\rm Leq}n)/I_n)^2$ compensates the dominate body effect distortion component $(-K1_n)/(16(2\Phi_{\rm fn}+V_{\rm OQ})^{3/2})$ in (11) is validated. As a consequence, the NSF displays better THD result than the PSF at a specific high frequency range. For CCSF, the THD is lower than that of the NSF because the n-channel body effect term is compensated by the p-channel body effect term via the optimized $V_{\rm OQ}$ in Fig. 9. Due to the potentially incomplete cancellation between the cross-product terms as observed in (18), the residual values that contribute to the THD will be higher than that of the PSF. This explains why the THD value lies between NSF and PSF, starting from a low frequency range. For high-frequency distortion compensation based on the design values of $\Delta V_n = 1.4$ V, $A_{{\rm bulk}\,n\_Q} = 1.48, C_{\rm Leq}n = 1.05$ pF, $I_n = 1$ mA, $\Delta V_p = 0.19$ V, $A_{{\rm bulk}\,p\_Q} = 1.2, C_{\rm Leq}p = 0.092$ pF, and $I_n = 0.1$ mA in the CCSF, it turns out that $(\Delta V_n A^{1/2}_{{\rm bulk}\,n\_Q})/(16)((\omega C_{\rm Leq}n)/I_n)^2 \cong (\Delta V_p A^{1/2}_{{\rm bulk}\,p\_Q})/(16)((\omega C_{\rm Leq}p)/I_p)^2$, and so the THD stays constant from low frequency to high frequency. This is different with NSF where low distortion optimization is based on compensation at a single frequency or PSF where the optimal low-frequency distortion is continuously degraded by increasing the frequency parameter. This also validates the proposed distortion optimized strategy for the frequency-independent pair using the optimized $V_{\rm OQ}$ and the frequency-dependent pair using balanced frequency-dependent term design as described in the CCSF analysis in (18).

For verification of the large-signal transfer functions, Fig. 11 compares the simulated frequency responses of the various

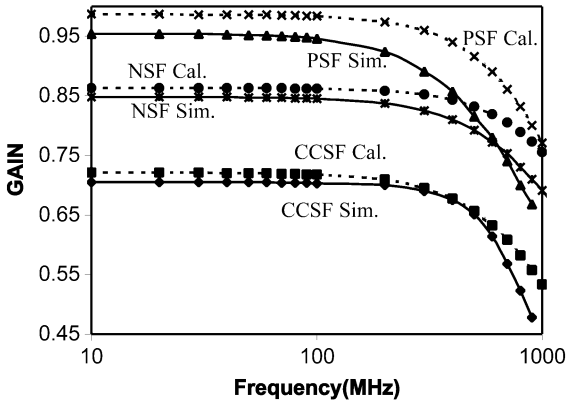

Fig. 11. Large-signal transfer function of various source followers at 1 $V_{\rm pp}$ input and 1 pF load.

source followers with the hand-calculated second-order analytical results. As in the simulated results, all the predicted curves show a rolling off characteristic at high frequencies but they also exhibit different low-frequency gain values. The low-frequency gain of PSF is much closer to the ideal case of unity. This is since the gain offset comes mainly from the channel length modulation terms which are relatively smaller than the nonlinear body effect terms in the NSF. The CCSF has displayed the lowest gain because of the summed body effects from both the NSF and PSF in the cascaded structure. This can be regarded as a limitation of the CCSF scheme which is subject to the values of the pMOS and nMOS process parameters.

The comparison of NSF, PSF and CCSF is summarized in Table III. All the schemes permit the optimized THD value to be less than 60 dB but with different frequency ranges. The CCSF offers the most significant optimized THD performance because it allows the circuit to operate with sustained low distortion in a wide frequency range. Nevertheless, the NSF offers the most bandwidth efficiency because the p-channel source followers limit the operation frequencies of both the PSF and CCSF. The discrepancies between the simulated and calculated results are mainly due to the use of simplified large-signal model (Fig. 2), simplified HSPICE BSIM3 model equations and because of the assumptions made for simplifying the derivation.

B. Case Study

In order to demonstrate the proposed optimization methodology, a case study is provided. Let us consider an example that uses the NSF design to illustrate the optimization. From (11), the THD of NSF is a function of process and design parameters. The design parameters can be used to achieve the primary optimization objectives. Since the quiescent output bias voltage $V_{\rm OQ}$ is set at half a supply voltage, the design parameters are identified as the biasing current I_n, effective capacitive load $C_{{\rm Leq}\,n}$, and angular signal frequency ω if the aspect ratio (see Table II) of the input transistor is fixed in ΔV_n.

To establish the relationship among the three parameters, the real portion from (11) is considered while the relatively small imaginary portion is neglected. Thus, (11) can be approximated as (24) shown at the bottom of the page. Note that $\mathrm{HD}_{2\_\mathrm{NSF}}$ is at a minimum when $\mathrm{HD}_{2\_\mathrm{NSF}} = 0$. Hence, the optimal angular frequency is approximated as (25) shown at the bottom of the page. It can be seen from (25) that the optimal angular frequency $\omega_{\rm opt}$ is proportional to the biasing current I_n whilst inversely proportional to the effective capacitive load $C_{{\rm Leq}\,n}$ if the effect of $\sqrt{(1/\Delta V_n)}$ is small. (25) will be used for circuit optimization, which can be demonstrated in the following specification cases.

Case 1) Find the optimal biasing current to achieve minimum distortion at frequency 50 MHz and a capacitive load of 1 pF.

Case 2) Find the optimal capacitive load to achieve minimum distortion at frequency 50 MHz and a biasing current of 1 mA.

Fig. 12(a) shows the THD under different biasing currents when the input frequency is 50 MHz and the capacitive load is 1 pF. Obviously, there is also an optimal biasing current for minimum THD. Fig. 12(b) shows the THD versus different output capacitive loads when the input frequency is 50 MHz and the biasing current is 1 mA. It is also observed that minimum THD is achieved at a particular capacitive load. By subtracting the optimal capacitive load with the output junction capacitances of NSF, the actual capacitive load C_L is obtained. Therefore, the optimization allows for the choice of appropriate biasing currents or capacitive loads such that an NSF design can be achieved with the optimized THD of less than -60 dB at dedicated high frequency.

C. Summary of Optimization Procedures

For the sake of design simplicity, the optimization procedures for the three source follower schemes are summarized. They will follow largely common procedures, but some aspects will be deviated to accommodate different nonlinear compensation mechanisms. The procedures are generalized as follows:

1) Obtain a large-signal model for a source follower circuit.
2) Establish relevant large-signal equations with the inclusion of dominant second-order effects.

$$\mathrm{HD}_{2\_\mathrm{NSF}} \cong \frac{\frac{-K1_n}{16(2\Phi_{\rm fn}+V_{\rm OQ})^{3/2}} + \frac{\Delta V_n A_{{\rm bulk}\,n\_Q}^{1/2}}{16}\left(\frac{\omega C_{{\rm Leq}\,n}}{I_n}\right)^2 + \frac{\Delta V_n K1_n A_{0n}}{32 A_{{\rm bulk}\,n\_Q}^{1/2}(2\Phi_{\rm fn}+V_{\rm OQ})^{5/2}}}{\left(1+\frac{K1_n}{2(2\Phi_{\rm fn}+V_{\rm OQ})^{1/2}}\right)^2} V_m \tag{24}$$

$$\omega_{\rm opt} \cong \frac{I_n}{C_{{\rm Leq}\,n}}\sqrt{\frac{K1_n}{A_{{\rm bulk}\,n\_Q}^{1/2}(2\Phi_{\rm fn}+V_{\rm OQ})^{3/2}}\left[\frac{1}{\Delta V_n} - \frac{A_{0n}}{2A_{{\rm bulk}\,n\_Q}^{1/2}(2\Phi_{\rm fn}+V_{\rm OQ})}\right]} \tag{25}$$

TABLE III
PERFORMANCE COMPARISON OF NSF, PSF, AND CCSF

Topology Condition: V_{dd} = 3V, Load = 1 pF and 1 V_{pp} input	NSF	PSF	CCSF
Frequency range for optimized THD < − 60dB at optimal V_{OQ}	Sim: 75–100MHz Cal: 90–110MHz	Sim: 0–35MHz Cal: 0–45MHz	Sim: 0–140MHz Cal: 0–160MHz
Low-frequency gain	Sim: 0.848 Cal: 0.863	Sim: 0.954 Cal: 0.987	Sim: 0.705 Cal: 0.721
Large-signal -3dB bandwidth	Sim: 1500 MHz Cal: 1800 MHz	Sim: 870 MHz Cal: 1170 MHz	Sim: 860 MHz Cal: 1100 MHz
Power consumption	3 mW	3 mW	3.3 mW

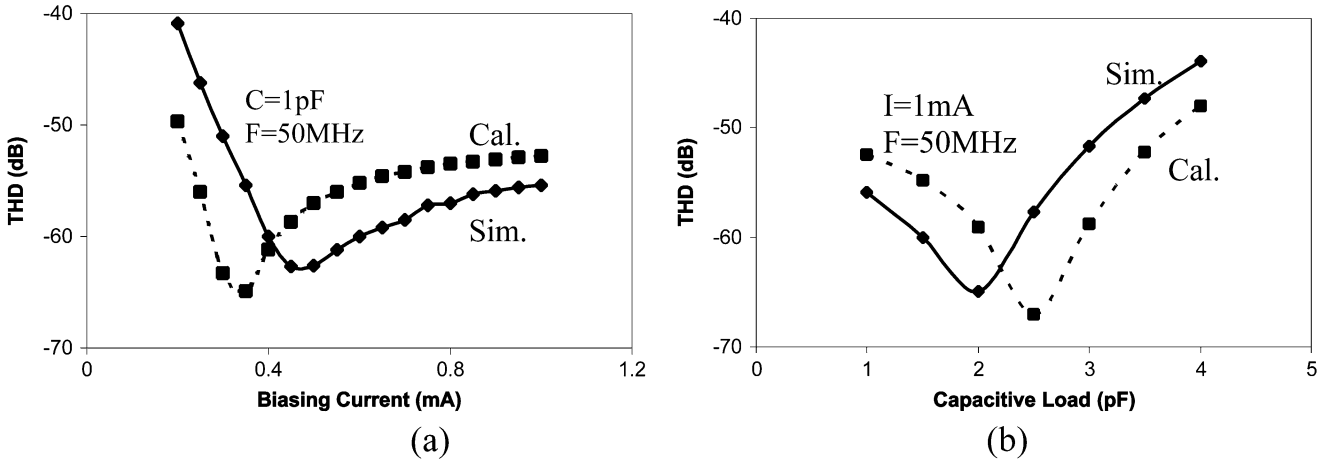

Fig. 12. THD optimization examples in NSF using: (a) biasing current and (b) capacitive load.

3) Analyze the input voltage of the circuit as a function of the output voltage in a second-order manner.
4) Derive the relevant coefficient expressions for the nonlinear output voltage.
5) Apply the HD_2 expression for the source follower using the standard definition (8).
6) Find the optimal V_{OQ} for each scheme to achieve low- frequency distortion compensation. Typically, $V_{OQ} = (1/2)V_{dd}$ for NSF due to no optimal point. Equate the bracketed expression $(4/P_{CLM\,p})(L_{1p\,eff})/(l_p)(E_{sat}L_{1p\,eff}\lambda_{1pQ})(\lambda_{1pQ}^2-\lambda_{2pQ}^2(\lambda_{2pQ})/(\lambda_{1pQ})(L_{2p\,eff}^2)/(L_{1p\,eff}^2)) + (\lambda_{2pQ}E_{sat}L_{2p\,eff})^2(3\lambda_{1pQ}^2(L_{1p\,eff})/(L_{2p\,eff}) - \lambda_{2pQ}^2) + (\lambda_{1pQ}E_{sat}L_{1p\,eff})^2(3\lambda_{1pQ}^2 - \lambda_{2pQ}^2(L_{2p\,eff})/(L_{1p\,eff}))$ to zero to find the optimized V_{OQ} for PSF since the channel length modulation factor λ is a function of V_{OQ} from (14). Use the dominant terms $(-K1_n)/(16(2\Phi_{fn}+V_{OQ})^{3/2})$ and $(K1_p)/(16[2\Phi_{fp} + (V_{DD}-V_{OQ}-V_{GS\_Q}-\Delta V_n)]^{3/2})$ to find the optimized V_{OQ} for CCSF.
7) Optimize for high-frequency distortion compensation. For NSF, find the approximate HD_2 expression and relate the relevant design parameters (see case study). For PSF, no further action is taken because there is no significant optimization in high frequency. For CCSF, balance the high-frequency terms, $(\Delta V_n A_{bulk\,n\_Q}^{1/2})/(16)((\omega C_{Leq\,n})\,/\,I_n)^2$ and $(-\Delta V_p A_{bulk\,p\_Q}^{1/2})\,/\,(16)((\omega C_{Leq\,p})/I_p)^2$.

V. CONCLUSION

The harmonic distortion of the conventional NSF and PSF are thorough analyzed using a simplified large-signal model in conjunction with Level 49 BSIM3 model equations and assumptions. Based on the analysis, a new linearization technique is proposed for the CCSF. In this technique, major distortion components that arise because of frequency independent or dependent effects can be minimized separately via one-to-one compensation in a complementary pair manner. Therefore, the CCSF can maintain rather high linearity with broad bandwidth. In addition, three new large-signal second harmonic equations are established together with transfer functions for three circuits. The distortion optimization strategy of each source follower is also proposed. A case study of NSF demonstrates the optimization example. A summary of the procedure is given to show the design steps for optimization. Comparative results have validated that the predicted results correlate well with the realistic HSPICE BSIM3 simulation results.

APPENDIX A
DETAILED DEVIATION OF HD_2 FOR NSF

$$V_i = f(V_o) = V_o + V_{th\,n0} + K1_n(\sqrt{2\Phi_{fn}+V_o} - \sqrt{2\Phi_{fn}}) + \Delta V_n\sqrt{A_{bulk\,n}\left[1+\frac{j\omega C_{Leq\,n}}{I_n}(V_o - V_{OQ})\right]}. \quad \text{(A-1)}$$

The coefficients, b_1 and b_2, are

$$\begin{aligned} b_1 &= f'(V_o = V_{\rm OQ}) = 1 + \frac{K1_n}{2(2\Phi_{\rm fn} + V_{\rm OQ})^{1/2}} \\ &\quad + \frac{\Delta V_n}{2A_{{\rm bulk}\,n\_Q}^{1/2}} \left(\frac{-K1_n A_{0n}}{4(2\Phi_{\rm fn} + V_{\rm OQ})^{3/2}} \right. \\ &\quad \left. + A_{{\rm bulk}\,n\_Q} \frac{j\omega C_{{\rm Leq}\,n}}{I_n} \right) \qquad \text{(A-2)} \\ b_2 &= \frac{f''(V_o = V_{\rm OQ})}{2} = \frac{-K1_n}{8(2\Phi_{\rm fn} + V_{\rm OQ})^{3/2}} \\ &\quad + \frac{\Delta V_n}{4} \left[\frac{-1}{2A_{{\rm bulk}\,n\_Q}^{3/2}} \left(\frac{K1_n A_{0n}}{4(2\Phi_{\rm fn} + V_{\rm OQ})^{3/2}} \right. \right. \\ &\quad \left. - A_{{\rm bulk}\,n\_Q} \frac{j\omega C_{{\rm Leq}\,n}}{I_n} \right)^2 \\ &\quad + \frac{1}{A_{{\rm bulk}\,n\_Q}^{1/2}} \left(\frac{3K1_n A_{0n}}{8(2\Phi_{\rm fn} + V_{\rm OQ})^{5/2}} \right. \\ &\quad \left. \left. - \frac{K1_n A_{0n}}{2(2\Phi_{\rm fn} + V_{\rm OQ})^{3/2}} \frac{j\omega C_{{\rm Leq}\,n}}{I_n} \right) \right]. \qquad \text{(A-3)} \end{aligned}$$

In (A-2)

$$\frac{\Delta V_n}{8A_{{\rm bulk}\,n\_Q}^{1/2}} \frac{K1_n A_{0n}}{(2\Phi_{\rm fn} + V_{\rm OQ})^{3/2}} \ll 1 + \frac{K1_n}{2(2\Phi_{\rm fn} + V_{\rm OQ})^{1/2}} \quad \text{and}$$
$$\frac{\Delta V_n}{2} A_{{\rm bulk}\,n\_Q}^{1/2} \frac{j\omega C_{{\rm Leq}\,n}}{I_n} \ll 1 + \frac{K1_n}{2(2\Phi_{\rm fn} + V_{\rm OQ})^{1/2}}$$

in the range of hundreds of megahertz. In (A-3)

$$\frac{-\Delta V_n}{16A_{{\rm bulk}\,n\_Q}^{3/2}} \left(\frac{K1_n A_{0n}}{4(2\Phi_{\rm fn} + V_{\rm OQ})^{3/2}} \right)^2$$

is smaller than other items. Finally, the second harmonic distortion can be expressed as (A-4) shown at the bottom of the page.

APPENDIX B
DETAILED DEVIATION OF $\rm HD_2$ FOR PSF

Please see (B-1) shown at the bottom of the page. The coefficients, b_1 and b_2, are

$$\begin{aligned} b_1 &= f'(V_o = V_{\rm OQ}) \\ &= 1 + \frac{\Delta V_p \sqrt{A_{{\rm bulk}\,p}}}{2} \left\{ \sqrt{\frac{1}{T_{2p} T_{1p}}} \left(\lambda_{2pQ}^2 E_{\rm sat} L_{2p\,\rm eff} \right. \right. \\ &\quad \left. \left. + \frac{j\omega C_{{\rm Leq}\,p}}{I_{p0}} \right) + \sqrt{\frac{T_{2p}}{T_{1p}^3}} \lambda_{1pQ}^2 E_{\rm sat} L_{1p\,\rm eff} \right] \right\} \qquad \text{(B-2)} \\ b_2 &= \frac{f''(V_o = V_{\rm OQ})}{2} \\ &= -\frac{\Delta V_p \sqrt{A_{{\rm bulk}\,p}}}{16} \left\{ \sqrt{\frac{1}{T_{2p}^3 T_{1p}}} \lambda_{2pQ}^4 E_{\rm sat}^2 L_{2p\,\rm eff}^2 \right. \\ &\quad - 2\sqrt{\frac{1}{T_{2p} T_{1p}^3}} \lambda_{1pQ}^2 \lambda_{2pQ}^3 E_{\rm sat}^2 L_{1p\,\rm eff} L_{2p\,\rm eff} \\ &\quad - 3\sqrt{\frac{T_{2p}}{T_{1p}^5}} \lambda_{1pQ}^4 E_{\rm sat}^2 L_{1p\,\rm eff}^2 + 4\sqrt{\frac{1}{T_{2p} T_{1p}}} \lambda_{2pQ}^3 \frac{E_{\rm sat} L_{2p\,\rm eff}^2}{P_{{\rm CLM}\,p} l_p} \\ &\quad - 4\sqrt{\frac{T_{2p}}{T_{1p}^3}} \lambda_{1pQ}^3 \frac{E_{\rm sat} L_{1p\,\rm eff}^2}{P_{{\rm CLM}\,p} l_p} + \sqrt{\frac{1}{T_{2p}^3 T_{1p}}} \left(\frac{j\omega C_{{\rm Leq}\,p}}{I_{p0}} \right)^2 \\ &\quad + 2\sqrt{\frac{1}{T_{2p}^3 T_{1p}}} \lambda_{2pQ}^2 E_{\rm sat} L_{2p\,\rm eff} \frac{j\omega C_{{\rm Leq}\,p}}{I_{p0}} \\ &\quad \left. - 2\sqrt{\frac{1}{T_{2p} T_{1p}^3}} \frac{j\omega C_{{\rm Leq}\,p}}{I_{p0}} \lambda_{1pQ}^2 E_{\rm sat} L_{1p\,\rm eff} \right\} \qquad \text{(B-3)} \end{aligned}$$

where $T_{2p} = 1 + \lambda_{2pQ}(V_{\rm DD} - V_{\rm OQ}), T_{1p} = 1 + \lambda_{1pQ} V_{\rm OQ}$. Note that $\lambda_{1pQ}, \lambda_{2pQ}$ are the constant values for λ_{1p} and λ_{2p}, respectively, when $V_o = V_{\rm OQ}$.

In (B-2)

$$\frac{\Delta V_p \sqrt{A_{{\rm bulk}\,p}}}{2} \left\{ \sqrt{\frac{1}{T_{2p} T_{1p}}} \left(\lambda_{2pQ}^2 E_{\rm sat} L_{2p\,\rm eff} + \frac{j\omega C_{{\rm Leq}\,p}}{I_{p0}} \right) \right.$$
$$\left. + \sqrt{\frac{T_{2p}}{T_{1p}^3}} \lambda_{1pQ}^2 E_{\rm sat} L_{1p\,\rm eff} \right] \right\} \ll 1$$

$$\begin{aligned} {\rm HD}_{2\_{\rm NSF}} &= \frac{1}{2} \frac{b_2}{b_1^2} \\ &\cong \frac{\frac{-K1_n}{16(2\Phi_{\rm fn} + V_{\rm OQ})^{3/2}} + \frac{\Delta V_n A_{{\rm bulk}\,n\_Q}^{1/2}}{16} \left(\frac{\omega C_{{\rm Leq}\,n}}{I_n} \right)^2 + \frac{\Delta V_n K1_n A_{0n}}{64 A_{{\rm bulk}\,n\_Q}^{1/2} (2\Phi_{\rm fn} + V_{\rm OQ})^{3/2}} \left[\frac{3}{(2\Phi_{\rm fn} + V_{\rm OQ})} - \frac{2j\omega C_{{\rm Leq}\,n}}{I_n} \right]}{\left[1 + \frac{K1_n}{2(2\Phi_{\rm fn} + V_{\rm OQ})^{1/2}} \right]^2} V_m \qquad \text{(A-4)} \end{aligned}$$

$$V_i = f_p(V_o) = V_o - V_{{\rm th}\,p0} - \Delta V_p \sqrt{\frac{A_{{\rm bulk}\,p}[1 + \lambda_{2p}(V_{\rm DD} - V_o)] - \frac{j\omega C_{{\rm Leq}\,p}}{I_{p0}}(V_o - V_{\rm OQ})}{1 + \lambda_{1p} V_o}} \qquad \text{(B-1)}$$

in the range of hundreds of MHz. Since $\lambda_{1pQ}, \lambda_{2pQ} \ll 1, T_{2p} \cong 1$ and $T_{1p} \cong 1$ in (B-3), the second harmonic distortion can be simplified as

$$\begin{aligned}
&\mathrm{HD}_{2_\mathrm{PSF}} \\
&\quad \cong \frac{1}{2}\frac{b_2}{b_1^2} \\
&\quad \cong \frac{\Delta V_p\sqrt{A_{\mathrm{bulk}\,p}}}{16} V_m \left\{ \frac{4}{P_{\mathrm{CLM}\,p}} \frac{L_{1p\,\mathrm{eff}}}{l_p} \right. \\
&\qquad \times (E_{\mathrm{sat}} L_{1p\,\mathrm{eff}} \lambda_{1pQ}) \left(\lambda_{1pQ}^2 - \lambda_{2pQ}^2 \frac{\lambda_{2pQ}}{\lambda_{1pQ}} \frac{L_{2p\,\mathrm{eff}}^2}{L_{1p\,\mathrm{eff}}^2} \right) \\
&\qquad + (\lambda_{2pQ} E_{\mathrm{sat}} L_{2p\,\mathrm{eff}})^2 \left(3\lambda_{1pQ}^2 \frac{L_{1p\,\mathrm{eff}}}{L_{2p\,\mathrm{eff}}} - \lambda_{2pQ}^2 \right) \\
&\qquad + (\lambda_{1pQ} E_{\mathrm{sat}} L_{1p\,\mathrm{eff}})^2 \left(3\lambda_{1pQ}^2 - \lambda_{2pQ}^2 \frac{L_{2p\,\mathrm{eff}}}{L_{1p\,\mathrm{eff}}} \right) \\
&\qquad + \left(\frac{\omega C_{\mathrm{Leq}\,p}}{I_{p0}} \right)^2 + 2\frac{j\omega C_{\mathrm{Leq}\,p}}{I_{p0}} E_{\mathrm{sat}} L_{1p\,\mathrm{eff}} \\
&\qquad \left. \times \left(\lambda_{1pQ}^2 - \lambda_{2pQ}^2 \frac{L_{2p\,\mathrm{eff}}}{L_{1p\,\mathrm{eff}}} \right) \right\}. \qquad \text{(B-4)}
\end{aligned}$$

Appendix C
Detailed Deviation of HD_2 for CCSF

$$\begin{aligned}
V_i = {} & V_o + V_{\mathrm{th}\,n0} + K1_n(\sqrt{2\Phi_{\mathrm{fn}} + V_o} - \sqrt{2\Phi_{\mathrm{fn}}}) \\
& + \Delta V_n \sqrt{A_{\mathrm{bulk}\,n}\left[1 + \frac{j\omega C_{\mathrm{Leq}\,n}}{I_n}(V_o - V_{\mathrm{OQ}})\right]} \\
& - V_{\mathrm{th}\,p0} - K1_p(\sqrt{2\Phi_{\mathrm{fp}} + [V_{\mathrm{DD}} - (V_o + V_{\mathrm{GS_}Q})]} \\
& - \sqrt{2\Phi_{\mathrm{fp}}}) \\
& - \Delta V_p \sqrt{A_{\mathrm{bulk}\,p}\left[1 - \frac{j\omega C_{\mathrm{Leq}\,p}}{I_p}(V_o + V_{\mathrm{GS_}Q} - V_{\mathrm{XQ}})\right]}
\end{aligned} \qquad \text{(C-1)}$$

with $V_{\mathrm{GS\_}Q} = V_{\mathrm{th}\,n0} + K1_n(\sqrt{2\Phi_{\mathrm{fn}} + V_{\mathrm{OQ}}} - \sqrt{2\Phi_{\mathrm{fn}}}) + \Delta V_n\sqrt{A_{\mathrm{bulk}\,n}}$. The coefficients, b_1 and b_2, are

$$\begin{aligned}
b_1 = f'(V_o = V_{\mathrm{OQ}}) = {} & 1 + \frac{K1_n}{2(2\Phi_{\mathrm{fn}} + V_{\mathrm{OQ}})^{1/2}} \\
& + \frac{K1_p}{2[2\Phi_{\mathrm{fp}} + (V_{\mathrm{DD}} - V_{\mathrm{OQ}} - V_{\mathrm{GS_}Q})]^{1/2}} \\
& - \frac{\Delta V_n}{8A_{\mathrm{bulk}\,n_Q}^{1/2}} \frac{K1_n A_{0n}}{(2\Phi_{\mathrm{fn}} + V_{\mathrm{OQ}})^{3/2}} \\
& - \frac{\Delta V_p}{8A_{\mathrm{bulk}\,p_Q}^{1/2}} \frac{K1_p A_{0p}}{[2\Phi_{\mathrm{fp}} + (V_{\mathrm{DD}} - V_{\mathrm{OQ}} - V_{\mathrm{GS_}Q})]^{3/2}} \\
& + \frac{\Delta V_n}{2} A_{\mathrm{bulk}\,n_Q}^{1/2} \frac{j\omega C_{\mathrm{Leq}\,n}}{I_n} + \frac{\Delta V_p}{2} A_{\mathrm{bulk}\,p_Q}^{1/2} \frac{j\omega C_{\mathrm{Leq}\,p}}{I_p}
\end{aligned} \qquad \text{(C-2)}$$

$$\begin{aligned}
b_2 = \frac{f''(V_o = V_{\mathrm{OQ}})}{2} = {} & \frac{-K1_n}{16(2\Phi_{\mathrm{fn}} + V_{\mathrm{OQ}})^{3/2}} \\
& + \frac{\Delta V_n}{8}\left[\frac{-1}{2A_{\mathrm{bulk}\,n_Q}^{3/2}} \left(\frac{K1_n A_{0n}}{4(2\Phi_{\mathrm{fn}} + V_{\mathrm{OQ}})^{3/2}} \right)^2 \right. \\
& \left. + \frac{3K1_n A_{0n}}{8A_{\mathrm{bulk}\,n_Q}^{1/2}(2\Phi_{\mathrm{fn}} + V_{\mathrm{OQ}})^{5/2}} \right] \\
& + \frac{\Delta V_n}{16} A_{\mathrm{bulk}\,n_Q}^{1/2} \left(\frac{\omega C_{\mathrm{Leq}\,n}}{I_n} \right)^2 \\
& + \frac{K1_p}{16[2\Phi_{\mathrm{fp}} + (V_{\mathrm{DD}} - V_{\mathrm{OQ}} - V_{\mathrm{GS_}Q})]^{3/2}} \\
& - \frac{\Delta V_p}{8}\left[\frac{-1}{2A_{\mathrm{bulk}\,p_Q}^{3/2}} \right. \\
& \times \left(\frac{K1_p A_{0p}}{4[2\Phi_{\mathrm{fp}} + (V_{\mathrm{DD}} - V_{\mathrm{OQ}} - V_{\mathrm{GS_}Q})]^{3/2}} \right)^2 \\
& \left. + \frac{3K1_p A_{0p}}{8A_{\mathrm{bulk}\,p_Q}^{1/2}[2\Phi_{\mathrm{fp}} + (V_{\mathrm{DD}} - V_{\mathrm{OQ}} - V_{\mathrm{GS_}Q})]^{5/2}} \right] \\
& - \frac{\Delta V_p}{16} A_{\mathrm{bulk}\,p_Q}^{1/2} \left(\frac{\omega C_{\mathrm{Leq}\,p}}{I_p} \right)^2 \\
& + \frac{\Delta V_n}{8}\left(\frac{-1}{4A_{\mathrm{bulk}\,n_Q}^{1/2}} \frac{K1_n A_{0n}}{(2\Phi_{\mathrm{fn}} + V_{\mathrm{OQ}})^{3/2}} \frac{j\omega C_{\mathrm{Leq}\,n}}{I_n} \right) \\
& - \frac{\Delta V_p}{8}\left(\frac{-1}{4A_{\mathrm{bulk}\,p_Q}^{1/2}} \right. \\
& \left. \times \frac{K1_p A_{0p}}{[2\Phi_{\mathrm{fp}} + (V_{\mathrm{DD}} - V_{\mathrm{OQ}} - V_{\mathrm{GS_}Q})]^{3/2}} \frac{j\omega C_{\mathrm{Leq}\,p}}{I_p} \right).
\end{aligned} \qquad \text{(C-3)}$$

In (C-2)

$$\begin{aligned}
& \frac{\Delta V_n}{8A_{\mathrm{bulk}\,n_Q}^{1/2}} \frac{K1_n A_{0n}}{(2\Phi_{\mathrm{fn}} + V_{\mathrm{OQ}})^{3/2}} \\
& \quad \frac{\Delta V_p}{8A_{\mathrm{bulk}\,p_Q}^{1/2}} \frac{K1_p A_{0p}}{[2\Phi_{\mathrm{fp}} + (V_{\mathrm{DD}} - V_{\mathrm{OQ}} - V_{\mathrm{GS_}Q})]^{3/2}} \ll 1 \\
& \frac{\Delta V_n}{2} A_{\mathrm{bulk}\,n_Q}^{1/2} \frac{j\omega C_{\mathrm{Leq}\,n}}{I_n}, \quad \frac{\Delta V_p}{2} A_{\mathrm{bulk}\,p_Q}^{1/2} \frac{j\omega C_{\mathrm{Leq}\,p}}{I_p} \ll 1
\end{aligned}$$

in the range of hundreds of megahertz. In (C-3)

$$\begin{aligned}
& \frac{-\Delta V_n}{16A_{\mathrm{bulk}\,n_Q}^{3/2}} \left(\frac{K1_n A_{0n}}{4(2\Phi_{\mathrm{fn}} + V_{\mathrm{OQ}})^{3/2}} \right)^2 \\
& \frac{-\Delta V_p}{16A_{\mathrm{bulk}\,p_Q}^{3/2}} \left(\frac{K1_p A_{0p}}{4[2\Phi_{\mathrm{fp}} + (V_{\mathrm{DD}} - V_{\mathrm{OQ}} - V_{\mathrm{GS_}Q})]^{3/2}} \right)^2
\end{aligned}$$

$$\mathrm{HD}_{2\_\mathrm{CCSF}} \cong \frac{1}{2}\frac{b_2}{b_1^2} \left\{ -\frac{K1_n}{16(2\Phi_{\mathrm{fn}}+V_{\mathrm{OQ}})^{3/2}} + \frac{\Delta V_n A_{\mathrm{bulk}\,n\_Q}^{1/2}}{16}\left(\frac{\omega C_{\mathrm{Leq}\,n}}{I_n}\right)^2 + \frac{\Delta V_n K1_n A_{0n}}{64 A_{\mathrm{bulk}\,n\_Q}^{1/2}(2\Phi_{\mathrm{fn}}+V_{\mathrm{OQ}})^{3/2}}\left(\frac{3}{(2\Phi_{\mathrm{fn}}+V_{\mathrm{OQ}})} - \frac{2j\omega C_{\mathrm{Leq}\,n}}{I_n}\right) + \frac{K1_p}{16[2\Phi_{\mathrm{fp}}+(V_{\mathrm{DD}}-V_{\mathrm{OQ}}-V_{\mathrm{GS\_}Q})]^{3/2}} - \frac{\Delta V_p A_{\mathrm{bulk}\,p\_Q}^{1/2}}{16}\left(\frac{\omega C_{\mathrm{Leq}\,p}}{I_p}\right)^2 - \frac{\Delta V_p K1_p A_{0p}}{64 A_{\mathrm{bulk}\,p\_Q}^{1/2}[2\Phi_{\mathrm{fp}}+(V_{\mathrm{DD}}-V_{\mathrm{OQ}}-V_{\mathrm{GS\_}Q})]^{5/2}}\left(\frac{3}{[2\Phi_{\mathrm{fp}}+(V_{\mathrm{DD}}-V_{\mathrm{OQ}}-V_{\mathrm{GS\_}Q})]} - \frac{2j\omega C_{\mathrm{Leq}\,p}}{I_p}\right) \right\} \Big/ \left\{1+\frac{K1_n}{2(2\Phi_{\mathrm{fn}}+V_{\mathrm{OQ}})^{1/2}} + \frac{K1_p}{2[2\Phi_{\mathrm{fp}}+(V_{\mathrm{DD}}-V_{\mathrm{OQ}}-V_{\mathrm{GS\_}Q})]^{1/2}}\right\}^2 V_m \tag{C-4}$$

are smaller than other items. Finally, the second harmonic distortion can be expressed as (C-4) shown at the top of the page.

REFERENCES

[1] M. A. M. Zin, H. Kobayashi, K. Kobayashi, and J. I. Ichimura, "A high-speed CMOS track/hold circuit," in *Proc. IEEE Int. Conf. Electronics, Circuits, and Systems (ICECS)*, vol. 3, Sep. 1999, pp. 1709–1712.

[2] Y. T. Wang and B. Razavi, "An 8-bit 150-MHz CMOS A/D converter," *IEEE J. Solid-State Circuits*, vol. 35, no. 3, pp. 308–317, Mar. 2000.

[3] K. Hadidi and A. Khoei, "A highly linear cascode-driver CMOS source follower buffer," in *Proc. IEEE Int. Conf. Electronics, Circuits, and Systems (ICECS)*, Oct. 1996, pp. 1243–1246.

[4] P. Wambacp and W. Sansen, *Distortion Analysis of Analog Integrated Circuits*. Norwell, MA: Kluwer , 1998.

[5] G. Palumbo and S. Pennisi, *Feedback Ampilfiers: Theory and Design*. Norwell, MA: Kluwer , Jan. 2002.

[6] G. Palumbo and S. Pennisi, "High-frequency harmonic distortion in feedback amplifiers: Analysis and applications," *IEEE Trans. Circuits Syst. I, Fundam. Theory Appl.*, vol. 50, no. 3, pp. 328–340, Mar. 2003.

[7] P. R. Gray, P. J. Hurst, S. H. Lewis, and R. G. Meyer, *Analysis and Design of Analog CMOS Integrated Circuits*. New York: Wiley, 2001.

[8] P. Cost, C. Fiocchi, U. Gatti, and F. Maloberti, "High-performance BiCMOS output buffer design strategies," in *Proc. IEEE Int. Symp. Circuits and Systems (ISCAS)*, vol. 2, May 1999, pp. 168–171.

[9] P. E. Allen and D. R. Holberg, *CMOS Analog Circuit Design*. Oxford, U.K.: Oxford Univ. Press, 2002.

[10] *Hspice User's Manual*, 2000. Meta-Software.

[11] P. Wambacq, G. Giles, and P. R. Kinget, "High-frequency distortion analysis of analog integrated circuits," *IEEE Trans. Circuits Syst. II, Analog Digit. Signal Process.*, vol. 46, no. 3, pp. 335–344, Mar. 1999.

[12] D. Johns and K. Martin, *Analog Integrated Circuit Design*. New York: Wiley, 1997.

[13] K. Simons, "The decibel relationship between amplifier distortion products," *Proc. IEEE*, vol. 58, no. 7, pp. 1071–1086, Jul. 1970.

[14] R. Meyer and A. Wong, "Blocking and desensitization in RF amplifier," *IEEE J. Solid-State Circuits*, vol. 30, no. 8, pp. 944–946, Aug. 1995.

[15] K. Hadidi, J. Sobhi, A. Hasankhaan, D. Muramatsu, and T. Matsumoto, "A novel highly linear CMOS buffer," in *Proc. IEEE Int. Conf. Electronics, Circuits, and Systems (ICECS)*, vol. 3, Sep. 1998, pp. 369–371.

Xianping Fan was born in China. She received both the Bachelor's and Master's degrees in electronic engineering from Xi'an Jiaotong University, Xi'an, China, in 1995 and 1998,respectively. Since August, 2000, she has been working toward the Ph.D. degree in the School of Electrical and Electronic Engineering, Nanyang Technological University (NTU), Singapore.

She worked as an Engineer in R&D center of Eastern Communication Company Limited, Hangzhou, China, from 1998 to 2000. Currently, she has joined O_2 Micro, Singapore as a Senior Design Engineer, with the responsibility for the mixed-signal IC design. Her research interests include circuit theory, integrated analog circuits and systems and high-speed analog–digital converter design and characterization.

P. K. Chan was born in Hong Kong. He received the B.Sc. (Hons.) degree from the University of Essex, Colchester, U.K., the M.Sc. degree from the University of Manchester, Institute of Science and Technology (U.M.I.S.T.), Manchester, U.K., and the Ph.D. degree from the University of Plymouth, Plymouth, U.K. in 1987, 1988, and 1992, respectively.

From 1989 to 1992, he was a Research Assistant with the University of Plymouth, working in the area of MOS continuous-time filters. In 1993, he joined the Institute of Microelectronics (IME) as a Member Technical Staff, where he designed CMOS sensor interfaces for industrial applications. In 1996, He was a Staff Engineer with Motorola, Singapore, where he developed the magnetic write channel for Motorola 1st generation hard-disk preamplifier. He joined Nanyang Technological University (NTU), Singapore, in 1997, where he is currently an Associate Professor in the School of Electrical and Electronic Engineering and Program Director [mixed-signal integrated circuit (IC) and applications] for the Center for Integrated Circuits and Systems (CICS). He holds four patents and is an IC Design Consultant to local and multinational companies in Singapore. He has also conducted numerous IC design short courses to the industrial companies and design centers. His research interests include circuit theory, amplifier frequency compensation techniques, sensing interfaces for integrated sensors, biomedical circuits and systems, integrated filters and data converters.